PHYSICAL REVIEW B **91**, 161101(R) (2015)

Analysis of the optical conductivity for A_2IrO_3 (A = Na, Li) from first principles

Ying Li,[1,*] Kateryna Foyevtsova,[2] Harald O. Jeschke,[1] and Roser Valentí[1]

[1]*Institut für Theoretische Physik, Goethe-Universität Frankfurt, Max-von-Laue-Strasse 1, 60438 Frankfurt am Main, Germany*

[2]*Quantum Matter Institute, University of British Columbia, Vancouver, British Columbia, Canada V6T 1Z4*

(Received 16 October 2014; revised manuscript received 13 January 2015; published 10 April 2015)

We present results for the optical conductivity of Na_2IrO_3 within density functional theory by including spin-orbit and correlation effects as implemented in the generalized gradient approximation. We identify the various interband transitions and show that the underlying quasimolecular-orbital nature of the electronic structure in Na_2IrO_3 translates into distinct features in the optical conductivity. Most importantly, the parity of the quasimolecular orbitals appears to be the main factor in determining strong and weak optical transitions. We also present optical conductivity calculations for α-Li_2IrO_3 and discuss the similarities and differences with Na_2IrO_3.

DOI: 10.1103/PhysRevB.91.161101 PACS number(s): 75.10.Jm, 71.70.Ej, 71.15.Mb

The family of honeycomb iridates A_2IrO_3 (A = Na, Li) has recently been a subject of intensive discussion due to its complex electronic and magnetic behavior arising from an interplay of spin-orbit effects, correlations, and lattice geometry. These materials are insulators and order antiferromagnetically at low temperatures [1]. While Na_2IrO_3 shows a zigzaglike magnetic pattern [2], a spiral order with a small nonzero wave vector inside the first Brillouin zone has been reported for α-Li_2IrO_3 [3,4]. Photoemission and optical conductivity measurements [5] for Na_2IrO_3 confirm this insulating behavior with a gap of 340 meV. Attempts to understand the different behavior of the end members through the series $(Na_{1-x}Li_x)_2IrO_3$ have been pursued [6,7] with partly contradicting results: While Manni *et al.* [6] find that only for $x \leqslant 0.25$ does the system form uniform solid solutions and otherwise the system shows a miscibility gap and phase separates, Cao *et al.* [7] report a homogeneous phase at $x \sim 0.7$ with a disappearance of long range magnetic order.

From a theoretical point of view, these materials have been suggested to be a realization of the Heisenberg-Kitaev model with bond-dependent anisotropic interactions between $j_{\text{eff}} = 1/2$ spin-orbit-coupled Ir moments [8–14]. Such a model is obtained under the assumption of large spin-orbit coupling, so that Ir $5d$ t_{2g} orbitals can be written in terms of $j_{\text{eff}} = 1/2$ and lower lying $j_{\text{eff}} = 3/2$ relativistic orbitals.

Alternatively, a description of the electronic structure of these systems in terms of quasimolecular orbitals was also recently proposed [15,16]. Following the observation that the contributing energy scales in these systems are of the same order of magnitude, namely, the bandwidth for $5d$ orbitals is 1.5–2 eV, the on-site Coulomb repulsion U is about 1–2 eV, the Hund's coupling constant is about 0.5 eV, and the spin-orbit (SO) coupling is $\lambda \sim 0.4$–0.5 eV, it was shown [15,16] that the underlying electronic behavior can be described in terms of molecular orbitals formed by the Ir t_{2g} states on a hexagon, with each of the three t_{2g} Ir orbitals on a site contributing to three neighboring molecular orbitals. In Ref. [16] it was further demonstrated that both descriptions, i.e., a localized description in terms of j_{eff} and an itinerant description in terms of molecular orbitals, are mutually compatible.

Presently, only optical conductivity $\sigma(\omega)$ measurements for Na_2IrO_3 are available [5,17]. $\sigma(\omega)$ in Na_2IrO_3 shows a broad peak structure at 1.5 eV [5] (1.66 eV in Ref. [17]) and smaller peak structures at 0.52, 0.72, 1.32, and 1.98 eV [17]. These features have been interpreted in terms of dominant $j_{\text{eff}} = 3/2$ and $j_{\text{eff}} = 1/2$ transitions [17]. With the aim of further unveiling the origin of different behavior in Na_2IrO_3 and α-Li_2IrO_3, we revisit the optical conductivity in Na_2IrO_3 with density functional theory calculations and show that the nature of the various interband transitions observed experimentally can be understood in terms of the parity of the underlying molecular-orbital description. In contrast, the optical conductivity behavior that we predict for α-Li_2IrO_3 shows an increase in weight at low energies with respect to Na_2IrO_3 due to a strong mixing of quasimolecular-orbital character, absent in Na_2IrO_3.

For our density functional theory (DFT) calculations we use the full-potential linearized augmented plane-wave (LAPW) method as implemented in the code WIEN2K [18]. The Perdew-Burke-Ernzerhof (PBE) generalized gradient approximation (GGA) [19] was employed as the exchange correlation functional and the basis-size controlling parameter $RK_{\max}$ was set to 8. A mesh of 450 $\mathbf{k}$ points in the first Brillouin zone (FBZ) for the self-consistency cycle was used. In order to have a good description of the experimentally observed optical gap in Na_2IrO_3, magnetism as well as a $U_{\text{eff}} = 2.4$ eV as implemented in GGA+U [20] had to be included in the calculations [21]. Relativistic effects were taken into account within the second variational approximation (GGA+SO+U). For the optical properties, we employed the optics code package [22] in WIEN2K. The optical properties were calculated with 1568 $\mathbf{k}$ points in the FBZ.

The imaginary part of the interband contribution to the dielectric function is given by [22,23]

$$\operatorname{Im}\epsilon_{\alpha\beta}(\omega) \propto \frac{1}{\omega^2}\sum_{c,v}\int d\mathbf{k}\,\langle c_{\mathbf{k}}|p^{\alpha}|v_{\mathbf{k}}\rangle\,\langle v_{\mathbf{k}}|p^{\beta}|c_{\mathbf{k}}\rangle \times \delta\left(\varepsilon_{c_{\mathbf{k}}} - \varepsilon_{v_{\mathbf{k}}} - \omega\right). \quad (1)$$

Here, α and β indicate directional components, p is the momentum operator, and ω corresponds to the energy of the photon. $c_{\mathbf{k}}$ denotes a state in the conduction band with the energy $\varepsilon_{c_{\mathbf{k}}}$ and $v_{\mathbf{k}}$ is a state in the valence band with the energy $\varepsilon_{v_{\mathbf{k}}}$. By absorbing photon energy, the electrons transit from $v_{\mathbf{k}}$

*Corresponding author: yingli@itp.uni-frankfurt.de

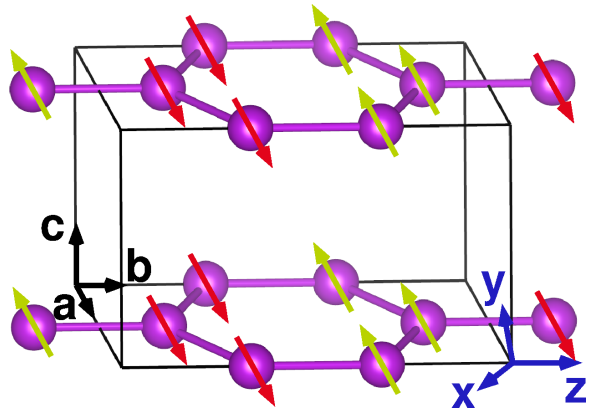

FIG. 1. (Color online) Ir honeycomb layers of Na_2IrO_3. The black axes **a**, **b**, and **c** are the vectors of the unit cell, while the dark blue axes **x**, **y**, **z** are the Cartesian axes. The red and green arrows show the zigzag AFM phase.

to $c_{\mathbf{k}}$. The real part of the dielectric function can be evaluated from the imaginary part using the Kramers-Kronig relation.

In this Rapid Communication we focus on the analysis of the real part of the optical conductivity,

$$\mathrm{Re}\,\sigma_{\alpha\beta}(\omega) = \frac{\omega}{4\pi}\mathrm{Im}\,\epsilon_{\alpha\beta}(\omega). \tag{2}$$

For our DFT analysis we used the experimental structure of Na_2IrO_3 given in Ref. [2], which agrees well with the relaxed structure [2,6], and performed GGA+SO+U ($U = 3$ eV, $J_{\mathrm{H}} = 0.6$ eV, $U_{\mathrm{eff}} = U - J_{\mathrm{H}} = 2.4$ eV) calculations in the zigzag antiferromagnetic (AFM) ordered phase (see Fig. 1) with the magnetization parallel to the **a** direction [24].

The density of states (DOS) and band structures for Na_2IrO_3 within GGA, GGA+SO, and GGA+SO+U are shown in Fig. 2. Compared to the nonrelativistic GGA DOS, a suppression of the DOS at E_{F} is clearly visible in the relativistic GGA+SO calculation. In GGA+SO+U, a 341 meV gap can be obtained, as reported experimentally [5]. Note that in the zigzag AFM phase there are four iridium atoms per unit cell and therefore the number of bands doubles to 12 t_{2g} in Fig. 2.

The monoclinic symmetry allows for four independent components of the optical conductivity tensor, defined as σ_{xx}, σ_{yy}, σ_{zz}, σ_{xy},

$$\begin{pmatrix} J_x \\ J_y \\ J_z \end{pmatrix} = \begin{pmatrix} \sigma_{xx} & \sigma_{xy} & 0 \\ \sigma_{xy} & \sigma_{yy} & 0 \\ 0 & 0 & \sigma_{zz} \end{pmatrix} \begin{pmatrix} E_x \\ E_y \\ E_z \end{pmatrix}. \tag{3}$$

The Cartesian directions are shown in Fig. 1. Here, **z** is parallel to the **b** direction and lies in the Ir hexagonal plane, while **x** and **y** are in the ac plane. Spin-orbit coupling also induces small nonzero contributions to the σ_{xz} and σ_{yz} components.

In Fig. 3(a), we present the calculated four dominant optical conductivity tensor components for Na_2IrO_3 in the low-frequency region. σ_{zz} corresponds to the dominant contribution to the in-plane optical conductivity and in Fig. 3(b) we compare this component with the experimental results [5,17] as well as with four-site iridium cluster calculations by Kim *et al.* [25]. Both our DFT calculations and the cluster calculations [25] show the presence of a dominant peak at

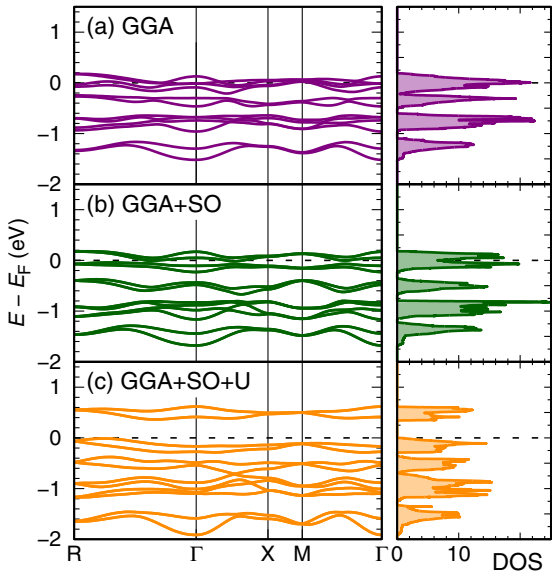

FIG. 2. (Color online) Ir 5d t_{2g} DOS and band structures for Na_2IrO_3 in zigzag magnetic order, obtained with (a) GGA, (b) GGA+SO, and (c) GGA+SO+U ($U = 3$ eV, $J_{\mathrm{H}} = 0.6$ eV, $U_{\mathrm{eff}} = U - J_{\mathrm{H}} = 2.4$ eV).

$\omega = 1.5$ eV, as observed in experiment. However, the DFT results have a richer structure and capture the multipeak behavior of the experimental observations.

In order to disentangle the origin of the various features present in the optical conductivity in Fig. 3(b), we display in Fig. 4 the various interband processes. For that purpose, we label in Fig. 4(a) the valence states v_s as a, b, c, d and the conduction states c_s as e. Note that the states denoted by c include twice the number of bands compared to the rest of the states. We identify four peaks in $\sigma(\omega)$ [Fig. 4(b)]; peaks A, B, C, D correspond to the transitions from a, b, c, d to e states, respectively. The analysis of the electronic structure in terms of quasimolecular orbitals [15,16] predicts a clear odd/even parity related to the symmetry of the quasimolecular orbitals, i.e., odd B_{1u}, even E_{1g}, odd E_{2u}, and even A_{1g}. Even though the zigzag magnetic order used for the calculations

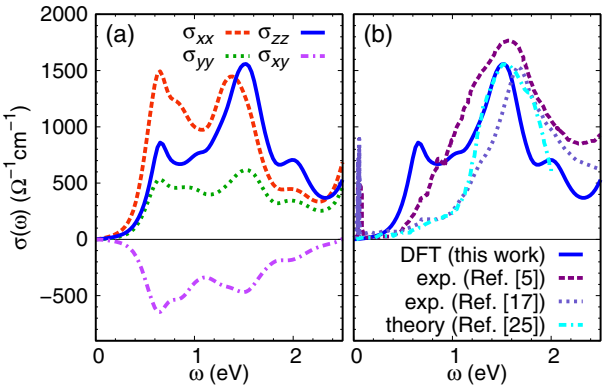

FIG. 3. (Color online) (a) Optical conductivity tensor components σ_{xx}, σ_{yy}, σ_{zz}, σ_{xy} and (b) DFT σ_{zz} for Na_2IrO_3 compared with experiment [5,17] and theory data [25].

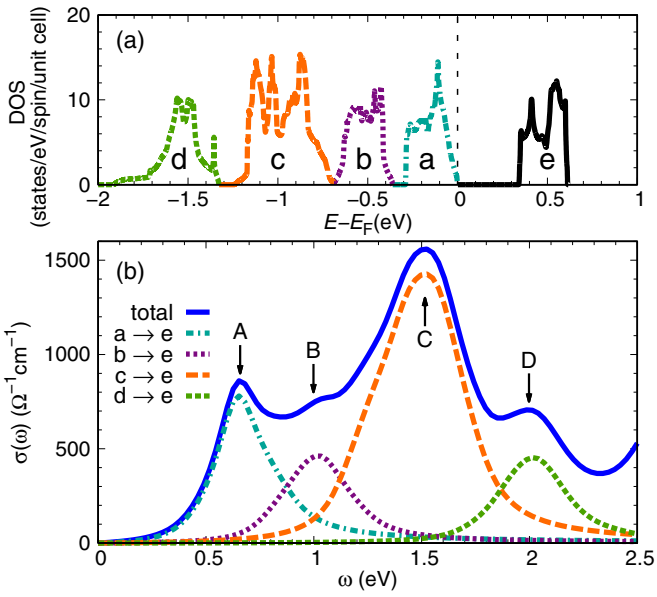

FIG. 4. (Color online) GGA+SO+U density of states (a) and contributions from different d-d transitions (b). The a, b, c, d, e label the five states.

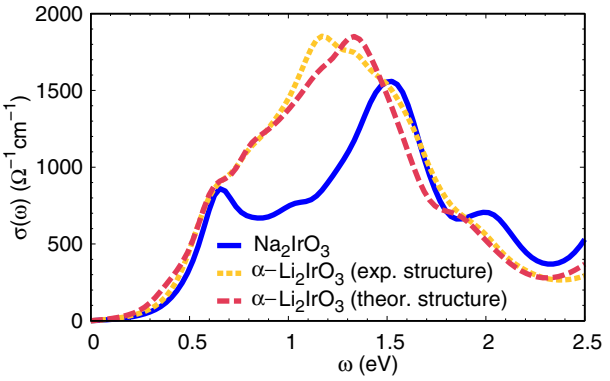

FIG. 5. (Color online) Comparison of the optical conductivity σ_{zz} between Na_2IrO_3 (experimental structure) and α-Li_2IrO_3 (experimental and theoretically predicted structure).

mixes states of different parities, we find in our analysis of the magnetic quasimolecular orbitals that the dominating parity contribution to a given state matches the parity of this state's counterpart in the paramagnetic phase. This, in particular, allows us to compare our spin-polarized calculations with the measurements performed above the magnetic transition temperature.

In the GGA+SO+U calculations we find that the states a, b, c, d, and e are predominantly of even, odd, even, odd, and odd parity, respectively. Since c contains twice the number of bands, we have an equal number of (predominantly) even and odd states, as expected for a parity conserving system; note that in the presence of spin-orbit coupling the states from the upper triad cannot be identified in terms of quasimolecular orbitals, however, we can still discern the dominant parity. Since the dielectric tensor matrix elements involved in the optical interband transitions are of the form $\langle v_s|\mathbf{E}\cdot\mathbf{r}|c_s\rangle$, with $\mathbf{E}\cdot\mathbf{r}$ being an odd parity operator, clearly, transitions between states of the same parity will be strongly suppressed whereas transitions between states of different parity will dominate. This is reflected in the large peak at 1.5 eV (peak C) that corresponds to a predominantly even to odd parity transition, followed by peak A (predominantly even to odd), while peaks B and D are of transitions between predominantly equal (odd) parity states and are strongly suppressed. The optical conductivity is therefore an important measure of the underlying molecular-orbital structure in Na_2IrO_3.

Before dealing with α-Li_2IrO_3, we would like to discuss the possible origin of the experimentally observed suppressed intensity of the peak centered at A with respect to the calculations. Possible sources of discrepancy could be (i) the fact that the optical conductivity was measured in the ab plane and σ tensor components other than σ_{zz} could influence the results. However, we estimated this contribution by averaging over the nonzero tensor components and found the effect to be very small. Another source of discrepancy may be (ii) effects not accounted for in the present DFT calculations, such as high-order contributions not included in linear response theory, or many-body effects beyond DFT such as excitonic states [26,27].

We now proceed with the calculation of the optical conductivity for α-Li_2IrO_3. The α-Li_2IrO_3 structure is known from powder x-ray diffraction [28] and from a careful DFT structure prediction using a spin-polarized GGA+SO+U exchange correlation functional [6]. As these two structures differ slightly and also show small but significant differences in electronic structure [29], we determine the optical conductivity for both of them. Experiments indicate that the gap of α-Li_2IrO_3 is of the same order of magnitude as in Na_2IrO_3 [28] or a bit smaller [30]. We find that magnetism and $U_{\text{eff}} = 2.4$ eV are necessary to open a gap of about 318 meV for the experimental structure while $U_{\text{eff}} = 2.0$ eV is necessary to open a gap of about 307 meV for the theoretical structure. Even though a spiral order has been suggested from experiment [3], we have considered, for simplicity, a zigzag magnetic order as in Na_2IrO_3 for the calculations. However, we checked the sensitivity of the optical conductivity to the type of magnetism by considering different (collinear) magnetic configurations (ferromagnetism, Néel, zigzag, stripy) and we found that the shape of the main peak centered at C is very robust and only the shapes of the peaks at A, B, and D show some changes. Therefore, we expect that the main features of the optical conductivity in α-Li_2IrO_3 calculated in the zigzag configuration provide a good description of α-Li_2IrO_3.

We compare the optical conductivities of Na_2IrO_3 and α-Li_2IrO_3 in Fig. 5. The energy integral of the optical conductivity in both cases is proportional to the effective number density of electrons. While the dominant peak in the Na_2IrO_3 optical conductivity is at 1.5 eV, we find it at 1.17 eV for the experimental structure and at 1.33 eV for the theoretical structure of α-Li_2IrO_3. Also, we observe an increase of the optical conductivity weight between 0.66 and 1.48 eV with respect to Na_2IrO_3. In order to analyze this behavior, we project the nonmagnetic GGA electronic structure of α-Li_2IrO_3 onto the quasimolecular-orbital basis (see Fig. 6). We observe that the separation of the density of states into isolated narrow bands of unique quasimolecular-orbital characters is much

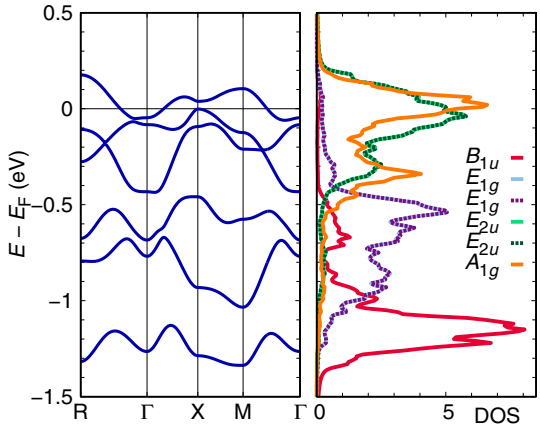

FIG. 6. (Color online) Nonrelativistic nonmagnetic band structure and density of states of the theoretically predicted α-Li_2IrO_3 structure, projected onto quasimolecular orbitals.

less clean than in Na_2IrO_3 [15,16] and resembles the case of Li_2RhO_3 [31]. In α-Li_2IrO_3, there is overlapping between B_{1u} and E_{1g} states and between E_{1g} and A_{1g}/E_{2u} states, as shown in Fig. 6. This strong mixing of character, which remains in the magnetic calculations, explains why the B peak in α-Li_2IrO_3 is much stronger than in Na_2IrO_3; the suppressed odd to odd transition in Na_2IrO_3 evolves into a mixture of enhanced and suppressed transitions in α-Li_2IrO_3.

We would like to emphasize that all the above DFT calculations have been performed with the inclusion of spin-orbit effects, and, strictly speaking, neither the t_{2g} (or the linear combination of t_{2g} states forming quasimolecular orbitals) nor spin are well-defined entities. Nevertheless, we have shown that the main features observed in optical conductivity are related to the underlying symmetries of the molecular-orbital basis, which is a manifestation of the fact that spin-orbit coupling is not the only determining interaction in these materials.

In summary, we have investigated the optical conductivity in Na_2IrO_3 and α-Li_2IrO_3 by performing magnetic GGA+SO+U calculations. Magnetism and a nonzero U were necessary in order to reproduce the experimental insulating gap in both systems. Using the fact that the narrow bands of Na_2IrO_3 are well described in terms of quasimolecular orbitals, we showed that the strength of the various interband contributions to the optical conductivity can be well described in terms of the parity of the quasimolecular orbitals, namely, weight suppression in like-parity transitions and weight enhancement in unlike-parity transitions. We also predict the shape of the optical conductivity for α-Li_2IrO_3. Contrary to Na_2IrO_3, in α-Li_2IrO_3 the quasimolecular orbitals strongly overlap and parities mix. This explains the relative weight differences in the optical conductivity between α-Li_2IrO_3 and Na_2IrO_3.

We would like to thank J. Orenstein, R. Coldea, J. Analytis, X. Xi, I. I. Mazin, and G. Khaliullin for very useful discussions. Y.L. acknowledges support through a China Scholarship Council (CSC) Fellowship. H.O.J and R.V. acknowledge support by the Deutsche Forschungsgemeinschaft through Grant No. SFB/TR 49.

[1] Y. Singh and P. Gegenwart, Phys. Rev. B **82**, 064412 (2010).
[2] S. K. Choi, R. Coldea, A. N. Kolmogorov, T. Lancaster, I. I. Mazin, S. J. Blundell, P. G. Radaelli, Y. Singh, P. Gegenwart, K. R. Choi, S.-W. Cheong, P. J. Baker, C. Stock, and J. Taylor, Phys. Rev. Lett. **108**, 127204 (2012).
[3] R. Coldea (unpublished).
[4] I. Kimchi, R. Coldea, and A. Vishwanath, arXiv:1408.3640.
[5] R. Comin, G. Levy, B. Ludbrook, Z.-H. Zhu, C. N. Veenstra, J. A. Rosen, Y. Singh, P. Gegenwart, D. Stricker, J. N. Hancock, D. van der Marel, I. S. Elfimov, and A. Damascelli, Phys. Rev. Lett. **109**, 266406 (2012).
[6] S. Manni, S. Choi, I. I. Mazin, R. Coldea, M. Altmeyer, H. O. Jeschke, R. Valentí, and P. Gegenwart, Phys. Rev. B **89**, 245113 (2014).
[7] G. Cao, T. F. Qi, L. Li, J. Terzic, V. S. Cao, S. J. Yuan, M. Tovar, G. Murthy, and R. K. Kaul, Phys. Rev. B **88**, 220414 (2013).
[8] G. Jackeli and G. Khaliullin, Phys. Rev. Lett. **102**, 017205 (2009).
[9] J. Chaloupka, G. Jackeli, and G. Khaliullin, Phys. Rev. Lett. **105**, 027204 (2010).
[10] Y. Yamaji, Y. Nomura, M. Kurita, R. Arita, and M. Imada, Phys. Rev. Lett. **113**, 107201 (2014).
[11] V. M. Katukuri, S. Nishimoto, V. Yushankhai, A. Stoyanova, H. Kandpal, S. Choi, R. Coldea, I. Rousochatzakis, L. Hozoi, and J. van den Brink, New J. Phys. **16**, 013056 (2014).
[12] J. G. Rau, E. K.-H. Lee, and H.-Y. Kee, Phys. Rev. Lett. **112**, 077204 (2014).
[13] J. Reuther, R. Thomale, and S. Rachel, Phys. Rev. B **90**, 100405(R) (2014).
[14] Y. Sizyuk, C. Price, P. Wölfle, and N. B. Perkins, Phys. Rev. B **90**, 155126 (2014).
[15] I. I. Mazin, H. O. Jeschke, K. Foyevtsova, R. Valentí, and D. I. Khomskii, Phys. Rev. Lett. **109**, 197201 (2012).
[16] K. Foyevtsova, H. O. Jeschke, I. I. Mazin, D. I. Khomskii, and R. Valentí, Phys. Rev. B **88**, 035107 (2013).
[17] C. H. Sohn, H.-S. Kim, T. F. Qi, D. W. Jeong, H. J. Park, H. K. Yoo, H. H. Kim, J.-Y. Kim, T. D. Kang, Deok-Yong Cho, G. Cao, J. Yu, S. J. Moon, and T. W. Noh, Phys. Rev. B **88**, 085125 (2013).
[18] P. Blaha, K. Schwarz, G. K. H. Madsen, D. Kvasnicka, and J. Luitz, *WIEN2k, An Augmented Plane Wave + Local Orbitals Program for Calculating Crystal Properties* (Karlheinz Schwarz, Techn. Universität Wien, Austria, 2001).
[19] J. P. Perdew, K. Burke, and M. Ernzerhof, Phys. Rev. Lett. **77**, 3865 (1996).
[20] V. I. Anisimov, I. V. Solovyev, M. A. Korotin, M. T. Czyzyk, and G. A. Sawatzky, Phys. Rev. B **48**, 16929 (1993).
[21] Please note that the U value used in density functional theory calculations depends on how the U term is implemented in the calculation. For example, FPLO (full potential local orbital code) can reproduce the experimental gap of 340 meV with $U = 1.1$ eV and $J = 0.5$ eV while WIEN2K needs $U_{\text{eff}} = 2.4$ eV.
[22] C. Ambrosch-Draxl and J. O. Sofo, Comput. Phys. Commun. **175**, 1 (2006).

[23] J. Ferber, Y.-Z. Zhang, H. O. Jeschke, and R. Valentí, Phys. Rev. B **82**, 165102 (2010).

[24] X. Liu, T. Berlijn, W.-G. Yin, W. Ku, A. Tsvelik, Y.-J. Kim, H. Gretarsson, Y. Singh, P. Gegenwart, and J. P. Hill, Phys. Rev. B **83**, 220403(R) (2011).

[25] B. H. Kim, G. Khaliullin, and B. I. Min, Phys. Rev. B **89**, 081109(R) (2014).

[26] E. Poem, Y. Kodriano, C. Tradonsky, N. H. Lindner, B. D. Gerardot, P. M. Petroff, and D. Gershoni, Nat. Phys. **6**, 993 (2010).

[27] S. Kilina, E. Badaeva, A. Piryatinski, S. Tretiak, A. Saxena, and A. R. Bishop, Phys. Chem. Chem. Phys. **11**, 4113 (2009).

[28] H. Gretarsson, J. P. Clancy, X. Liu, J. P. Hill, E. Bozin, Y. Singh, S. Manni, P. Gegenwart, J. Kim, A. H. Said, D. Casa, T. Gog, M. H. Upton, H.-S. Kim, J. Yu, V. M. Katukuri, L. Hozoi, J. van den Brink, and Y.-J. Kim, Phys. Rev. Lett. **110**, 076402 (2013).

[29] See Supplemental Material at http://link.aps.org/supplemental/10.1103/PhysRevB.91.161101 for the effect of broadening, the electronic structure for α-Li_2IrO_3, and the optical conductivity of α-Li_2IrO_3 resolved for different d-d transitions.

[30] M. Jenderka, R. Schmidt-Grund, M. Grundmann, and M. Lorenz, J. Appl. Phys. **117**, 025304 (2015).

[31] I. I. Mazin, S. Manni, K. Foyevtsova, H. O. Jeschke, P. Gegenwart, and R. Valentí, Phys. Rev. B **88**, 035115 (2013).